The challenge and benefit of using sea ice concentration satellite data products with uncertainty estimates in summer sea ice data assimilation

Q. Yang[1,2], M. Losch[2], S. Losa[2], T. Jung[2,3], L. Nerger[2], T. Lavergne[4]

1. National Marine Environmental Forecasting Center, Beijing, China
2. Alfred Wegener Institute, Helmholtz Centre for Polar and Marine Research, Bremerhaven, Germany
3. University of Bremen, Bremen, Germany
4. Norwegian Meteorological Institute, Oslo, Norway

Correspondence to: Q. Yang (Qinghua.Yang@awi.de)

Abstract

Data assimilation experiments that aim at improving summer ice concentration and thickness forecasts in the Arctic are carried out. The data assimilation system used is based on the MIT general circulation model (MITgcm) and a local Singular Evolutive Interpolated Kalman (LSEIK) filter. The effect of using sea ice concentration satellite data products with appropriate uncertainty estimates is assessed by three different experiments using sea ice concentration data of the European Space Agency Sea Ice Climate Change Initiative (ESA SICCI) which are provided with a per-grid cell physically based SIC uncertainty estimate. The first experiment uses the constant uncertainty, the second one imposes provided SICCI uncertainty estimate, while the third experiment employs an elevated minimum uncertainty to account for a representation error. Using the observation uncertainties that are provided with the data improves the ensemble mean forecast of ice concentration compared to using constant data errors, but ice thickness forecast is degraded. Further investigating this lack of positive impact on the sea ice thicknesses leads us to a fundamental mismatch between the satellite-based radiometric concentration and the modelled physical ice concentration in summer: the passive microwave sensors used for deriving the vast majority of the sea ice concentration satellite-based observations, cannot distinguish ocean water (in leads) from melt water (in ponds). New data assimilation methodologies that fully account or mitigate this mismatch must be designed for successful assimilation of sea ice concentration satellite data in summer melt conditions. In our study, thickness forecasts can be slightly improved by adopting the pragmatic solution of raising the minimum observation uncertainty, to inflate the data error and ensemble spread.

1. Introduction

For the past 30 years, the Arctic sea ice extent and volume consistently decreased in all seasons with a maximum decline in summer (Vaughan et al., 2013). This retreat has large effects on the climate system. For example, the strong contrast between the albedo of sea ice and open water has a profound effect on the Arctic surface heat budget. This retreat also influences the lower-latitude weather and climate, and has been linked to extreme events at mid-latitudes, for example, unusually cold and snowy winters in Europe, the US and Eastern Asia (Liu et al., 2012; Cohen et al., 2012), heat waves and droughts in the US and in Europe (Tang et al., 2014) and anomalous anticyclone circulation over eastern European and Russia (e.g., Semmler et al., 2012; Yang and Christensen, 2012). Apart from its relevance to regional and global climate, Arctic sea ice decline opens new economic opportunities. Accurate summer sea ice forecasts are therefore urgently required to thoroughly manage the opportunities (e.g., shipping, tourism) and risks (e.g., oil spill, marine emergencies) associated with Arctic opening (Eicken, 2013).

Sea ice data assimilation (DA) plays a pivotal role in sea ice forecasting, as it can provide realistic initial model states, and continuously constrain the model state closer to reality. Data assimilation requires both reliable observed quantities and realistic uncertainty estimates. These requirements, especially regarding data uncertainties, are now also increasingly recognized by the sea ice remote sensing community. Previous studies have shown that the assimilation of sea ice concentration data can improve sea ice concentration estimates (e.g., Lisæter et al., 2003; Lindsay and Zhang, 2006; Stark et al., 2008; Tietsche et al., 2013; Buehner et al., 2014) and also constrain the ice thickness and volume (Schweiger et al., 2011; Yang et al., 2015a). Given that error

estimates in the studies mentioned above were assumed to be constant, there is scope for further improvement through the use of more realistic uncertainty estimates.

In 2010, the European Meteorological Satellite Agency (EUMETSAT) Ocean and Sea Ice Satellite Application Facility (OSISAF, www.osi-saf.org) released a climate data record of sea ice concentration based on SMMR and SSM/I data (Eastwood et al., 2011; Product OSI-409). This dataset features an explicit correction of the satellite signal due to weather contamination, dynamic adaptation of algorithm tie-points, and spatio-temporally varying maps of uncertainties. In fact, this OSI-409 dataset and its uncertainties were already successfully used for data assimilation purposes (e.g., Massonnet et al. 2013).

In May 2014, the European Space Agency (ESA)-Sea Ice Climate Change Initiative (SICCI) released a sea ice concentration data set with associated uncertainty estimates (Version 1.11) to the public. In many respects, the SICCI sea ice concentration dataset features an update of the algorithms and processing methodologies used for the OSISAF OSI-409 dataset and, importantly, revised uncertainty estimates (Lavergne and Rinne, 2014). At the time of writing these two datasets, SICCI and OSISAF OSI-409, are the only algorithms or products that come with a physically based sea ice retrieval uncertainty information - as opposed to an estimate of the spatio-temporal variation of the ice concentration within a certain grid area and time window (e.g., NOAA SIC CDR, Peng et al., 2013). This new data set SICCI (v1.11) provides an opportunity to study the effect of the revised local (i.e., spatially varying) uncertainties on the assimilation of sea ice concentration data, and hence sea ice prediction skill.

In this study, we follow the approach of Yang et al. (2015a) and Yang et al. (2015b) by focusing on the summer of 2010 and using the same ensemble-based Singular Evolutive Interpolated Kalman (SEIK) filter (Pham et al., 1998; Pham, 2001) in its local form (LSEIK, Nerger et al., 2006). The SEIK filter algorithm is selected to assimilate the sea ice concentration because it is computationally efficient when applied to nonlinear models (Nerger et al., 2005), and a localized implementation of such a filter allows for more detailed sampling of forecast uncertainties (Nerger et al., 2006). The LSEIK filter has already been successfully used for the sea ice concentration data assimilation (Yang et al., 2015a). The purpose of the study is to quantify the impact of different observational uncertainty approximations on sea ice data assimilation through a comparison with independent ice concentration and ice thickness observations.

2. Forecasting experiment design

We use the MITgcm sea ice-ocean model (Marshall et al., 1997; Losch et al., 2010; Losch et al., 2014). Following Yang et al. (2015a) and Yang et al. (2015b), this study employs an Arctic regional configuration with a horizontal resolution of about 18 km and open boundaries in the North Atlantic and North Pacific (Losch et al., 2010; Nguyen et al., 2011). To explicitly include flow dependent uncertainty in atmospheric forcing, the approach by Yang et al. (2015a) was used in which UK Met Office (UKMO) ensemble forecasts from the TIGGE archive (THORPEX Interactive Grand Global Ensemble) drive the ensemble of sea ice-ocean models. Each of the selected UKMO ensemble forecasts consists of one unperturbed 'control' forecast and an ensemble of 23 forecasts with perturbed initial conditions. For further details the reader is referred to Bowler et al. (2008) and Yang et al. (2015a).

Following Yang et al. (2015a) and Yang et al. (2015b), the system's forecasting skills are evaluated with a series of 24h forecasts over the period of 1 June to 30 August 2010 during which the LSEIK filter is applied every day. This particular period is chosen as it was the first time that the open water was found in the interior pack ice near the North Pole as early as 12 July 2010 (NSIDC, http://nsidc.org/arcticseaicenews/2010/07/). During this summer melting period the Arctic sea ice extent (area with at least 15% sea ice concentration) shrank from 11.8 million km^2 on 1 June to 5.2 million km^2 on 30 August 2010 (ftp://sidads.colorado.edu/pub/DATASETS/NOAA/G02135/north/daily/data/, accessed on December 12, 2015), which shows a clear picture of sea ice melting in Arctic summer: on 1 June, most of the Arctic Ocean was covered with closed ice pack, while on 30 August, the sea ice area was shrunk to the central Arctic and the concentration was drastically reduced (Fig. 1).

The simulated and satellite observed sea ice concentration are combined using a sequential SEIK filter with second order exact sampling (Pham et al., 1998; Pham, 2001) coded within the Parallel Data Assimilation Framework (PDAF, Nerger and Hiller, 2013; http://pdaf.awi.de). The filter algorithm includes the following phases: initialization, forecast, analysis and ensemble transformation. The sequence of forecast, analysis and ensemble transformation is repeated.

The required initial ensemble approximates the uncertainty in the initial state of the physical phenomena. Following Losa et al. (2012) and Yang et al. (2015a), we used a model integration driven by the 24-h UKMO control forecasts over the period of 1 June to 31 August 2010 to estimate the initial state error covariance matrix of sea ice concentration and thickness. The leading Empirical Orthogonal Functions (EOFs) of this covariance matrix representing the model variability are transformed by the second-order exact sampling to generate the initial ensemble of ice concentration and thickness. An ensemble size of 23 states is chosen to match with the ensemble size of UKMO perturbed forcing. In the forecast phase, all ensemble states are dynamically evolved in time with the fully nonlinear sea ice model driven by the UKMO ensemble atmospheric forcing. The analysis step *k* combines the predicted model state x_k^f with the observational information y_k and computes a corrected state x_k^a every 24 hours as following.

$$x_k^a = x_k^f + K_k\left(y_k - H_k x_k^f\right)$$

$$K_k = P_k^f H_k^T (H_k P_k^f H_k^T + R_k)^{-1}$$

Here *K* is the so-called Kalman gain that weights the observational information based on the model and data error covariance, P_k^f and R_k respectively. H_k is the observational operator that project the model variable to the observational space. In the analysis step the error covariance matrix and ensemble of model state approximating the P_k^a are updated. With the SEIK filter as a reduced-rank square-root approach, the updated ensemble of model states samples the analyzed model uncertainties according to the leading EOFs. As seen from the formulas the quality of the analysis and, therefore, the system's prediction skills depend on the assumed prior error statistics P_k and R_k . In this respect it is worth stressing the importance of accounting for representativeness/representation errors. Such errors relate to uncertainties in the projection of model variables to the observational space. This could be any discrepancy in the used observational operator, for instance due to the fact that the model and data could represent the observed variable on different temporal and spatial scales or the model variable is not directly relates to the observation. There are also deficiencies in approximating and sampling the model uncertainties. In practice, it is rather difficult to estimate a priori the representation error also due to the conditional nature of error statistics specified in data assimilation algorithms. Thus computationally it may lead to some necessity to enlarge observational uncertainties.

In Nerger et al. (2006) it was shown that implementation of the SEIK analysis in a local context (LSEIK) allows for a more accurate approximation of the forecast error covariance given still a relatively small ensemble size. Thus, in our study the LSEIK analysis is performed for each water column of the model surface grid by assimilating the observational information only within a radius of 126 km (~7 model grid points). Within the radius, we weighted the observations assuming quasi-Gaussian (Gaspari and Cohn, 1999) dependence of the weights on the distance from the analyzed grid point (see Janjić et al., 2012, Losa et al., 2012). As the atmospheric errors are already explicitly accounted for by the ensemble forcing, an ensemble inflation simulating model errors is not needed in this LSEIK configuration (Yang et al., 2015a).

Two daily sea ice concentration data sets are used in this study. The SICCI fields from AMSR-E (Lavergne and Rinne, 2014) are used in the data assimilation. This product consists of daily fields provided on a 25 km polar-centered EASE2 grid (Brodzick et al. 2012). In the SICCI data set, the North Pole data gap is filled by interpolation, and daily maps of total standard error (the sum of algorithm uncertainties and smear uncertainties which refers to the representative error on a different grid resolution) are provided. If the provided concentration

product is effected by and the uncertainties contain the smearing error the data assimilative system accounts for this. The ice concentration data used for comparison are from the National Snow and Ice Data Center (NSIDC; Cavalieri et al. 1984). This product also consists of daily fields with 25 km grid spacing on a polar stereographic projection. For summer 2010, the NSIDC ice concentration fields are derived from a different passive microwave instrument (SSMIS onboard DMSP F-17) and with a different algorithm (NASA-Team). In summary, these products have two main differences: One is that these are on different Earth grids (polar stereographic versus EASE2). The second is that AMSR-E has a finer native spatial resolution than SSMI/S, therefore although both products are provided on a 25 km grid the SICCI (AMSR-E based) show more details and appear less smoothed than NSIDC (SSMI/S based), especially in the sea ice edge area (Figure 1). Strictly speaking, these differences do not make the SICCI and NSIDC products independent data, because both are derived from passive microwave instruments, but we may assume that they are sufficiently different for to be treated as independent.

Currently, there are some satellite-based observations of ice thickness, e.g., ICESat (Kwok et al., 2009), CryoSat-2 (Laxon et al., 2013; Zygmuntowska et al., 2014), and SMOS (Tian-Kunze et al., 2014), but currently it is generally impossible to retrieve reliable sea ice thickness from either laser/radar altimetry or brightness temperature during summer melt conditions due to wet snow conditions and or clouds. There is also no available sea ice thickness data from Operation Ice Bridge (OIB) in this summer as the OIB campaign only acts in spring (Kurtz et al., 2013). Instead of satellite and air-born based remote-sensing data we compare our simulation results to in-situ measurements of sea ice draft from the Beaufort Gyre Exploration Project (BGEP) Upward Looking Sonar (ULS) moorings located in the Beaufort Sea (BGEP_2009A, BGEP_2009D; see Fig. 1a for the locations) and sea ice thickness data obtained from autonomous ice mass balance buoys (IMBs; Perovich et al., 2013). The error in ULS measurements of ice draft is estimated as 0.1 m (Krishfield and Proshutinsky, 2006). To facilitate a direct comparison with the model ice thickness, following Vinje et al. (1998) and Hansen (2013), the drafts are converted to thickness by multiplying by a factor of 1.136. This constant ratio between thickness and draft was derived by Vinje and Finnekili (1986) through hand drillings. Different ice types and ice densities have different effects on the draft-thickness conversion by introducing uncertainties and nonlinear relationships between thickness and the original drafts (Forsström et al., 2011), however, these effects are just simply ignored in this study. The IMBs use two acoustic rangefinders to monitor the position of the ice bottom and the snow/ice surface, and estimate the sea-ice thickness. The accuracy of both sounders is 5mm (Richter-Menge and others, 2006). In this study, the IMB_2010B were used; its trajectories during summer 2010 are shown in Figure 1.

Three experiments, which mainly differ in the way observational uncertainties are represented, form the backbone of this study:

1. LSEIK-1: Following Yang et al. (2015a), SICCI sea ice concentration data are assimilated with a constant uncertainty value of 0.25, i. e., the observation errors are assumed to be Gaussian distributed with standard deviations (STD) of 0.25, including representation errors.
2. LSEIK-2: Same as LSEIK-1 but using the uncertainty fields provided with the SICCI product (see Figure 2). A minimum uncertainty of 0.01 is imposed to avoid complications due to divisions by very small numbers.
3. LSEIK-3: Same as LSEIK-2, but with a minimum uncertainty of 0.10 to account for a possible representation error. To account for the aforementioned representation error that is difficult to estimate a priori. We also have tested some other values (0.05, 0.15, 0.20) as case studies. The results of 0.05 are very close to the results of 0.01 value, the results of 0.20 are very close to the 0.25 constant uncertainties, while the results of 0.10 fall between the results of 0.05 and 0.20. So the value of 0.10 is chosen here to show the comparison with the experiment using the provided uncertainty.

To reflect the increased uncertainty in the extrapolation of the SICCI data into the data-void North Pole region, a constant uncertainty of 0.30 is assigned in this region for all experiments.

The original observational data uncertainties of ice concentrations that are provided with the SICCI data set and used in LSEIK-2 and LSEIK-3 are displayed in Figure 2. In Fig 2, we show the provided observation uncertainties on 12 July, 20 July, 13 August and 21 August 2010. The uncertainties are about 0.05 over packed ice and open water, but larger uncertainties up to and beyond 0.3 are present at the ice edge, and regions of

intermediate ice concentration values. The SICCI total uncertainties are indeed the sum of two components, one characterizing the algorithm uncertainties, and the other measuring the uncertainties due to representativity of 25 km daily averages, geo-location and instrument foot-print mismatch (Lavergne and Rinne, 2014). The second component to the total uncertainties is only pronounced in areas of gradients in the sea ice concentration observations – typically at the ice edge,– and amount for the inability of such coarse resolution satellite observations to accurately locate sea ice edge. Should the SICCI sea ice concentrations be assimilated in models with significantly better spatial resolution, the enlarged uncertainties allow the model to freely locate its ice edge within the 25×25 km grid cells showing intermediate ice concentration values in the data.

3. Results

Figure 3 shows the effect of assimilating SICCI concentration data on the simulated sea-ice concentration averaged over August 2010 (Fig. 3b, 3c and 3d). The model free-run strongly overestimated sea-ice concentrations in the surrounded sea ice area and lower estimated the sea ice concentration in the central Arctic, while the three LSEIK experiments well corrected the model bias towards observed values. Furthermore, the LSEIK-2 which uses the originally SICCI-provided uncertainties gives the best agreement with the SICCI observations.

Figure 4 compares the root mean square error (RMSE) for ensemble mean ice concentration forecasts with and without data assimilation with respect to the assimilated SICCI (Fig. 4a) and the non-assimilated NSIDC (Fig. 4b) ice concentration for the period 1 June to 30 August 2010. Note that Fig. 4 shows only the RMSE for grid locations where the satellite products reports an ice concentration lower than 0.35. These are thus mostly locations along the ice edge. Although this chosen threshold (0.35) is a bit arbitrary, but the trend of RMSE evolutions for a threshold of 0.25 and 0.50 are similar with the results of 0.35. Fig. 4 thus mostly assesses how the data assimilation experiments constrain the envelope of Arctic sea ice (cyan color around concentrations of 0.35 in Fig. 1), not the interior. The reason for choosing this range is that all sea ice concentration products from passive microwave instruments have challenges with high concentration values in the summer (Ivanova et al., 2015). In such a case, documenting that the assimilated state is closer to the NSIDC product is not very conclusive, since NSIDC and SICCI products are probably likewise challenged at high concentration values. Looking away from the ice concentration values and focusing on the outskirt of the sea ice cover make the conclusions somewhat more robust as the influence of melt-ponds is reduced, and the approaches over open water are different in both products. For example, the explicit weather correction method used in the SICCI product does not correct for cloud liquid water and cannot eliminate all weather influences on the ice concentration. In contrast the weather filter used for the NSIDC data cuts off sea ice concentration at various values (Ivanova et al., 2015). It should be also noted that for this comparison, the observations are linearly interpolated to the model grid. Such interpolation could lead to small local changes in sea ice concentration, and the related biases are not discussed in this study.

All the data assimilation experiments reduce deviations of the forecasted ice concentration from the satellite-based data sets. The RMSE temporal evolutions are associated with the number of available data points that can be used for comparison or with surface forcing. The curves of MITgcm free-runs differ between Fig. 4a and Fig. 4b because the RMSE is calculated with different sea ice concentration data sets. Compared to the free run without data assimilation, mean RMSE of LSEIK-1, LSEIK-2 and LSEIK-3 ensemble mean forecasts with respect to the SICCI data are reduced from on average, 0.56 to 0.18, and 0.07, 0.16, respectively. Similarly, the RMSE with respect to the NSIDC data are reduced from 0.55 to 0.20, 0.13 and 0.19. At all times, LSEIK-2 and LSEIK-3, using the SICCI-provided uncertainty estimates and adjusted minimum uncertainties, agree better with both the assimilated SICCI and non-assimilated NSIDC observations than LSEIK-1, which employs a constant uncertainty of 0.25. Again, it is worth pointing out that LSEIK-2, with the originally SICCI-provided uncertainties, agrees best with both SICCI and NSIDC observations. This shows that for this summer, the forecasting system produces an ensemble mean state for sea ice concentration that agrees better with the two ice concentration data sets when the full range of uncertainties provided by the SICCI satellite observation is used.

Nevertheless, the forecasts of sea ice thickness in LSEIK-2 are hardly realistic. Figure 5c shows an unrealistically noisy sea ice thickness forecast for experiment LSEIK-2 on 30th of August.

The time series of daily 24-hr forecast of sea ice thickness are compared to in-situ ULS-observations BGEP_2009A (Fig. 6a) and BGEP_2009D (Fig. 6b). Note, that the numerical model carries mean thickness (volume over area) as a variable. The observed thickness is multiplied by SICCI or NSIDC local ice concentration to arrive at the observed ULS-SICCI or ULS-NSIDC grid-cell mean thicknesses shown in Fig. 6. Although there are some small differences between ULS-SICCI or ULS-NSIDC, both reveal a very similar variation: at BGEP_2009A, the grid-cell mean thickness on 1 June was about 2.5m. With ice melting, the thickness was rapidly reduced in July, and reached about 0.2m on 30 August (Fig. 6a). Similarly, the grid-cell mean thickness at BGEP_2009D was about 3.5m on 1 June and was reduced to less than 0.1m on 30 August (Fig. 6b). All forecasts with data assimilation show improvements over the free-running MITgcm after late July when the misfit between the observed and modeled sea ice concentrations becomes significant (Figure not shown). This is because the ice thickness is influenced by the data assimilation only through the covariances between the ice concentration and thickness (Yang et al., 2015a). The ice thickness RMSE with respect to ULS-SICCI at BGEP_2009A has been reduced from 0.86m in the free model run to 0.43m in LSEIK-1, 0.61m in LSEIK-2, and 0.43 m in LSEIK-3 (Table 1). Similarly, the RMSE with respect to ULS-SICCI at BGEP_2009D has been reduced from 0.93m in the free model run to 0.55m in LSEIK-1, 0.51m in LSEIK-2, and 0.59m in LSEIK-3 (Table 1). By using the original SICCI uncertainty, LSEIK-2 gives a good agreement with the in-situ observations at BGEP_2009D (Fig. 6b), but over-estimates the mean sea ice thickness at BGEP_2009A (Fig. 6a), especially from mid-July to mid-August. By imposing a minimum uncertainty of 0.10 in the original uncertainties, the LSEIK-3 thickness agrees better with the BGEP_2009A data, and is basically equivalent to LSEIK-1.

The ice thickness at IMB 2010B (Figure 6d) has only ten data points in the period 6 June to 8 August, because its snow sounder failed on 7 May. Similarly, the observed thickness is multiplied by SICCI or NSIDC local ice concentration to arrive at the observed IMB-SICCI or IMB-NSIDC grid-cell mean thicknesses shown in Fig. 6. All the 24 h forecasts have a positive bias of about 1.0 m on 6 June. However, all the three LSEIK forecasts capture the downward trend after 11 July better than the free-running model, in particular, the LSEIK-3 gives the best agreement with the observations. The RMSEs from the IMB-SICCI at IMB 2010B are reduced from 0.91 m to 0.54 m with LSEIK-1, 0.73 m with LSEIK-2 and to 0.51 m with LSEIK-3. The reason is discussed in the following section.

4. Discussion

Based on the recently released SICCI sea ice concentration data that provides uncertainty estimates, a series of sensitivity experiments with different data error statistics have been carried out to test the impact of sea ice concentration uncertainties in data assimilation. Compared to a data assimilation configuration with constant uncertainty of 0.25, the data assimilation of SICCI data with provided uncertainties can give a better short-range ensemble mean forecasts for sea ice concentration in summer. But the ice thickness forecasts is not improved with the observational uncertainties. As there is still no available satellite based sea ice thickness data in summer, the ice thickness evaluation in this study are only based on two local ULS and one IMB based observations. Also because we calculate the grid-cell mean sea ice thickness using the local SICCI or NSIDC sea ice concentration data and certainly has potential bias, this introduces further uncertainties to the thickness calculations.

The main message from Figure 3 and 4 is in fact that the high sensitivity of the data assimilation to the observation uncertainties can be explained by the employed (atmospheric) model and observational error statistics in the LSEIK assimilation system. Although we have not directly included the model errors due to the possible suboptimal sea ice internal parameters, the ensemble forcing approach used here was shown to be very effective at representing model uncertainty associated with atmospheric forcing fields (Yang et al. 2015a). In fact, more reliable information on the prior model and observational error statistics increases the realism of the time evolution of the posterior forecast error statistics, which are approximated by the ensemble of model trajectories.

The spread of the ensemble representing forecast uncertainties in sea ice concentration for LSEIK-2 turns out to be relatively small. For example, on 30 August 2010, most of the ensemble-represented STDs in the Arctic

central area and the sea ice edge area are less than 0.01 and 0.03, respectively (Fig. 7b). This means that all members are very close to the ensemble mean and the data assimilation will have only little effect. Comparing LSEIK-2, LSEIK-3 has a similar spatial distribution of the ensemble spared with higher STDs in the sea ice edge area and lower STDs in the concentrated central ice area but overall higher STDs. Together with the fact that LSEIK-2 does not fit the thickness observations as well as LSEIK-3, this suggests that the ensemble forecast spread for sea ice concentration is too low and cannot reflect the true uncertainty. As only observations of sea ice concentration are assimilated, sea ice thickness is influenced indirectly during the data assimilation through the point-wise covariance between the ice concentration and thickness, thus through a linear update. Here, the very small sea ice concentration ensemble variance leads to a very small sea ice thickness spread (Fig. 8b). This probably explains why the LSEIK-2 system is not very effective at improving the sea ice thickness estimates while LSEIK-3 does somewhat better. The increased ensemble spread in the sea ice concentration allows the system to better represent the uncertainties and leads to a larger ice thickness spread (Fig. 8c). The sea ice thickness forecasts are improved accordingly.

The relative enhanced skill of sea ice thickness forecasts by LSEIK-3 with respect to LSEIK-2, does thus point to a possible issue with assimilating the summer SICCI ice concentration with the provided uncertainties. At first sight, the data uncertainties in summer sea ice pack seem to be too low (Fig. 2). For example, on 12 July 2010 when surface ice melting prevails and the microwave radiometry based ice concentration estimates are known to underestimate the physical sea ice cover (Ivanova et al., 2015), the provided uncertainties at the sea ice pack area are still lower than 0.06 with few regions exhibiting values around 0.1 (Fig. 2d).

In fact, Ivanova et al., (2015, section 5.3 "Melt ponds") report that AMSR-E and SSM/I, like all other passive microwave sensors, cannot distinguish ocean water (in leads) from melt water (in ponds) because of the very shallow penetration depths of the microwave signal in water. Therefore, these radiometric sea ice concentrations are closer to one minus the open water fraction (ponds and leads), than to the physical sea ice concentration in our models. This mismatch between the observed and modelled ice concentration (radiometric vs. physical) does not exist in winter when there is no surface melting. But in summer melt conditions, the observed ice concentration includes an unknown area of pond water. For example, the MODIS based melt pond distribution data clearly show the common distribution of melt ponds over the Arctic sea ice (middle panels in Fig. 9), and the passive microwave based sea ice concentration are underestimated in the pond covered area. The provided uncertainties are not larger since the radiometric concentration is not more uncertain. This mismatch results in a systematic difference between the two quantities (the physical concentration is larger than the radiometric concentration) that cannot be fully mitigated by enlarged standard deviations of a Gaussian uncertainty model in Ivanova et al. (2015). The influence of melt-ponds on the accuracy of the SICCI dataset is documented in Lavergne and Rinne (2014, section 2.2.1.1 "summer melt-ponding").

The left panels of Figure 9 show the bias in the SIC model prediction relative to the observation on 12 July, 20 July, 13 August and 21 August, 2010, the spatial distribution of the melt pond fraction (middle panels in Fig. 9) further supports that the data assimilative system performs more realistically when the prior observational error statistics account for some representativeness errors as in experiment LSEIK-3.

This mismatch between the measured and modelled quantities calls for adopting more advanced data assimilation methodologies, e.g. embedding a matching relation in form of an observation operator, that would necessarily include modelled melt pond fraction, for successful assimilation of sea ice concentration satellite observations (from passive microwave instruments). Given the scope of this study and the comparisons with the in-situ BGEP and IMB ice thickness, the solution implemented in LSEIK-3, that is to enlarge the observation uncertainties using a minimum value of 0.10, is a pragmatic but effective approach. This simple approach can well reflect the larger uncertainties in the sea ice edge area with a more reasonable ensemble spread and agree better with the observation given the information on the melt pond fractions.

5. Conclusion

In this study, we assimilate the summer SICCI sea ice concentration data taking into account the data uncertainties provided by the distributors. Even with a constant data uncertainty for the SICCI data, comparing

the assimilated SICCI and non-assimilated NSIDC ice concentration and BGEP/IMB in-situ thickness data, its assimilation results in better estimates of the sea ice concentration and thickness. The sea ice concentration estimates are further improved when the SICCI-provided uncertainty estimates are taken into account, but the sea ice thickness cannot be improved.

Moreover, it was found that our data assimilation system cannot give a reasonable ensemble spread of sea ice concentration and thickness if we use the provided uncertainty directly. This is because 1) there is a mismatch between the summer sea ice concentration as observed by the passive microwave sensors (radiometric concentration) and that simulated by our model (physical concentration), and 2) the provided observation uncertainties do not account for this mismatch. A simple and pragmatic approach appears to bypass this by imposing a minimum threshold value on the provided uncertainties in summer. Fully resolving the mismatch calls for more research, for example by considering melt-pond cover and evolution in the models or observation operators in the data assimilation schemes. That would allow one to reduce the representation error. Nevertheless, the part of error related to possible uncertainties in the approximation of the forecast error statistics and discrepancies in model and data up- or downscaling may still exist and has to be considered in any data assimilation algorithm.

Acknowledgements

We thank ESA's Sea Ice Climate Change Initiative (SICCI; http://icdc.zmaw.de/projekte/esa-cci-sea-ice-ecv0.html) and the National Snow and Ice Data Center (NSIDC; http://nsidc.org/data/docs/daac/nsidc0051_gsfc_seaice.gd.html) for providing the ice concentration data, the Woods Hole Oceanographic Institution (http://www.whoi.edu/beaufortgyre) for the provision of sea ice draft, the Cold Regions Research and Engineering Laboratory (http://imb.erdc.dren.mil/) for IMB data, and the Integrated Climate Data Center (http://icdc.zmaw.de) of University of Hamburg for the melt pond fraction data. The UKMO ensemble forecasting data were accessed through the TIGGE data server in European Centre for Medium-Range Weather Forecasts (ECMWF; http://tigge.ecmwf.int). This study is supported by the BMBF (Federal Ministry of Education and Research, Germany) - SOA (State Oceanic Administration, China) Joint Project (01DO14002) and the National Natural Science Foundation of China (41376005, 41376188). We thank the editor and two anonymous reviewers for constructive comments that helped improve the manuscript.

References

Bowler, N., Arribas, A., Mylne, K., Robertson, K., Beare, S.: The MOGREPS short-range ensemble prediction system. Q. J. R. Meteorol. Soc., 134: 703–722, doi: 10.1002/qj.234, 2008.

Brodzik, M. J., Billingsley, B.,, Haran, T., Raup, B., Savoie, M. H.: EASE-Grid 2.0: Incremental but Significant Improvements for Earth-Gridded Data Sets. ISPRS International Journal of Geo-Information, 1(1):32-45, doi:10.3390/ijgi1010032, 2012.

Buehner, M., Caya, A., Carrieres, T., Pogson, L.: Assimilation of SSMIS and ASCAT data and the replacement of highly uncertain estimates in the Environment Canada Regional Ice Prediction System, Q. J. R. Meteorol. Soc., doi:10.1002/qj.2408, 2014.

Cavalieri, D. J., Gloersen, P., and Campbell, W. J.: Determination of sea ice parameters with the NIMBUS 7 SMMR, J. Geophys. Res., 89, 5355–5369, 1984.

Cohen, J. L., Furtado, J. C., Barlow, M. A., Alexeev, V. A., and Cherry, J. E.: Arctic warming, increasing snow cover and widespread boreal winter cooling, Environ. Res. Lett., 7 (1), 014007, 2012.

Comiso, J. C.: Characteristics of Arctic winter sea ice from satellite multispectral microwave observations, J. Geophys. Res., 91(C1): 975-994, doi: 10.1029/JC091iC01p00975, 1986.

Eastwood, S., Larsen, K. R., Lavergne, T., Neilsen, E. and Tonboe, R.: OSI SAF global sea ice concentration reprocessing: product user manual, version 1.3. EUMETSAT OSI SAF (Product 0SI-409), 2011.

Eicken, H.: Ocean science: Arctic sea ice needs better forecasts, Nature, 497(7450), 431-433, 2013.

Forsström, S., Gerland, S., and Pedersen, C. A.: Thickness and density of snow-covered sea ice and hydrostatic equilibrium assumption from in situ measurements in Fram Strait, the Barents Sea and the Svalbard coast, Ann. Glaciol., 52(57), 261–270, 2011.

Gaspari, G., and Cohn, S. E.: Construction of correlation functions in two and three dimensions, Quart. J. Roy. Meteor. Soc., 125(554), 723-757, 1999.

Hansen, E., Gerland, S., Granskog, M. A., Pavlova, O., Renner, A. H. H., Haapala, J., Løyning, T. B, and Tschudi M.: Thinning of Arctic sea ice observed in Fram Strait: 1990-2011, J. Geophys. Res. Oceans, Vol. 118, doi: 10.1002/jgrc.20393, 2013.

Ivanova, N., Pedersen, L. T., Tonboe, R. T., Kern, S., Heygster, G., Lavergne, T., Sørensen, A., Saldo, R., Dybkjær, G., Brucker, L., and Shokr, M.: Inter-comparison and evaluation of sea ice algorithms: towards further identification of challenges and optimal approach using passive microwave observations, The Cryosphere, 9, 1797-1817, 2015, doi: 10.5194/tc-9-1797-2015.

Janjić, T., Nerger, L., Albertella, A., Schröter, J., Skachko, S.: On domain localization in ensemble based Kalman filter algorithms, Mon. Weather Rev., 139, 2046–2060, 2011.

Kern, S., Khvorostovsky, K., Skourup, H., Rinne, E., Parsakhoo, Z. S., Djepa, V., Wadhams, P., and Sandven, S.: The impact of snow depth, snow density and ice density on sea ice thickness retrieval from satellite radar altimetry: results from the ESA-CCI Sea Ice ECV Project Round Robin Exercise, The Cryosphere, 9, 37-52, doi:10.5194/tc-9-37-2015, 2015.

Krishfield, R. and Proshutinsky, A.: BGOS ULS Data Processing Procedure Report, http://www.whoi.edu/fileserver.do?id=85684pt=2p=100409, Woods Hole Oceanographic Institute, 2006.

Kurtz, N. T., Farrell, S. L., Studinger, M., Galin, N., Harbeck, J. P.,Lindsay, R., Onana, V. D., Panzer, B., and Sonntag, J. G.: Sea ice thickness, freeboard, and snow depth products from Operation IceBridge airborne data, The Cryosphere, 7, 1035–1056, doi:10.5194/tc-7-1035-2013, 2013.

Kwok, R. and Rothrock, D.: Decline in Arctic sea ice thickness from submarine and ICESat records: 1958–2008, Geophys. Res. Lett., 36, L15501, doi:10.1029/2009GL039035, 2009.

Lavergne, T. and Rinne, E.: Sea Ice Climate Change Initiative Phase 1: D3.4 Product User Guide (PUG), version 2.0. Ref: SICCI-PUG-13-07, 2014.

Laxon, S. W., Giles, K. A., Ridout, A. L., Wingham, D. J., Willatt, R., Cullen, R., Kwok, R., Schweiger, A., Zhang, J., Haas, C., Hendricks, S., Krishfield, R., Kurtz, N., Farrell, S. and Davidson, M. (2013), CryoSat-2 estimates of Arctic sea ice thickness and volume, Geophys. Res. Lett., 40, 732–737, doi:10.1002/grl.50193, 2013.

Lindsay, R. W. and Zhang, J.: Assimilation of ice concentration in an ice-ocean model, J. Atmos. Oceanic Technol., 23(5), 742-749, 2006.

Lisæter, K. A., Rosanova, J. and Evensen, G.: Assimilation of ice concentration in a coupled ice–ocean model, using the Ensemble Kalman filter, Ocean Dyn., 53(4), 368-388, 2003.

Liu, J., Curry, J. A., Wang, H., Song, M., and Horton, R. M.: Impact of declining arctic sea ice on winter snowfall, Proc. Natl. Acad. Sci. U.S.A., 109(11):4074-9., doi: 10.1073/pnas.1114910109, 2012.

Losa, S., Danilov, S., Schröter, J., Nerger, L., Maßmann, S., and Janssen, F.: Assimilating NOAA SST data into the BSH operational circulation model for the North and Baltic Seas: Inference about the data, J Marine. Syst., 105-08, 152-162, 2012.

Losch, M., Menemenlis, D., Campin, J. M., Heimbach, P. and Hill, C.: On the formulation of sea-ice models. Part 1: Effects of different solver implementations and parameterizations, Ocean Modell., 33(1), 129-144, 2010.

Losch, M., Fuchs, A., Lemieux, J., and A. Vanselow: A parallel Jacobian-free Newton-Krylov solver for a coupled sea ice-ocean model, J. Comp. Phys., 257(A), 901-911, doi:10.1016/j.jcp.2013.09.026, 2014.

Marshall, J., Adcroft, A., Hill, C., Perelman, L. and Heisey, C.: A finite-volume, incompressible Navier Stokes model for studies of the ocean on parallel computers, J. Geophys. Res., 102(C3), 5753-5766, 1997.

Massonnet, F., Mathiot, P., Fichefet, T., Goosse, H., König Beatty, C., Vancoppenolle, M., and Lavergne, T.: A model reconstruction of the Antarctic sea ice thickness and volume changes over 1980–2008 using data assimilation, Ocean Modell., 64, 67-75, 2013.

Nerger, L., Hiller, W. and Schröter, J.: A comparison of error subspace Kalman filters, Tellus A, 57(5), 715-735, 2005.

Nerger, L., Danilov, S., Hiller, W. and Schröter, J.: Using sea-level data to constrain a finite-element primitive-equation ocean model with a local SEIK filter, Ocean Dyn., 56(5-6), 634-649, 2006.

Nerger, L. and Hiller, W.: Software for ensemble-based data assimilation systems—Implementation strategies and scalability, Comp. & Geosci., 55, 110-118, 2013.

Nguyen, A. T., Menemenlis, D. and Kwok, R.: Arctic ice-ocean simulation with optimized model parameters: Approach and assessment, J. Geophys. Res., 116(C4), C04025, doi:10.1029/2010JC006573, 2011.

Peng, G., Meier, W. N., Scott, D. J., and Savoie, M. H.: A long-term and reproducible passive microwave sea ice concentration data record for climate studies and monitoring, Earth Syst. Sci. Data, 5, 311-318, doi:10.5194/essd-5-311-2013, 2013.

Perovich, D.K., Richter-Menge, J.A., Elder, B., Arbetter, T., Claffey, K., and Polashenski, C.: Observing and understanding climate change: Monitoring the mass balance, motion, and thickness of Arctic sea ice. http://imb.erdc.dren.mil/, 2013 (accessed 15 December 2013).

Pham, D. T., Verron, J., and Gourdeau, L.: Singular evolutive Kalman filters for data assimilation in oceanography, C. R. Acad. Sci. Paris, Earth Planet. Sci. , 326, 255-260, 1998.

Pham, D.: Stochastic methods for sequential data assimilation in strongly nonlinear systems, Mon. Weather Rev. 129: 1194–1207, 2001.

Richter-Menge, J. A., Perovich, D. K., Elder, B.C., Claffey, K., Rigor, I. and Ortmeyer, M.: Ice mass balance buoys: a tool for measuring and attributing changes in the thickness of the Arctic sea-ice cover. Ann. Glaciol., 44, 205–210, doi: 10.3189/172756406781811727, 2006.

Rothrock, D. A., Percival, D. B., and Wensnahan, M. : The decline in arctic sea-ice thickness: Separating the spatial, annual, and interannual variability in a quarter century of submarine data, J. Geophys. Res., 113, C05003, doi:10.1029/2007JC004252, 2008.

Schweiger, A., Lindsay, R., Zhang, J., Steele, M., Stern, H., and Kwok, R.: Uncertainty in modeled Arctic sea ice volume, J. Geophys. Res., 116, C00D06, doi:10.1029/2011JC007084, 2011.

Semmler, T., McGrath, R., and Wang, S.: The impact of Arctic sea ice on the Arctic energy budget and on the climate of the Northern mid-latitudes, Clim. Dyn., 39, 2675–2694, doi:10.1007/s00382-012-1353-9, 2012.

Smith, D. M. Extraction of winter total sea-ice concentration in the Greenland and Barents Sea from SSM/I data, Int. J. Remote Sens., 17(3): 2625–2646, doi: 10.1080/01431169608949096, 1996.

Stark, J. D., Ridley, J., Martin, M. and Hines, A.: Sea ice concentration and motion assimilation in a sea ice−ocean model, J. Geophys. Res., 113(C5), C05S91, doi:10.1029/2007JC004224, 2008.

Tang, Q., Zhang, X., and Francis, J. A.: Extreme summer weather in northern midlatitudes linked to a vanishing cryosphere, Nature Clim. Change, 4 (1): 45–50, 2014.

Tian-Kunze, X., Kaleschke L., Maaß N., Mäkynen M., Serra N., Drusch M., and Krumpen T.: SMOS-derived thin sea ice thickness: algorithm baseline, product specifications and initial verification, The Cryosphere, 8, 997-1018, doi:10.5194/tc-8-997-2014, 2014.

Tietsche, S., Notz, D., Jungclaus, J., and Marotzke, J.: Assimilation of sea-ice concentration in a global climate model- physical and statistical aspects, Ocean Sci. 9(1): 19-36, 2013.

Vaughan, D.G., Comiso, J.C., Allison, I., Carrasco, J., Kaser, G., Kwok, R., Mote, P., Murray, T., Paul, F, Ren, J., Rignot, E., Solomina, O., Steffen, K. and Zhang, T. : Observations: Cryosphere. In: Climate Change 2013: The Physical Science Basis. Contribution of Working Group I to the Fifth Assessment Report of the Intergovernmental Panel on Climate Change [Stocker, T.F., Qin, D., Plattner, G.-K., Tignor, M., Allen, S.K., Boschung, J., Nauels, A., Xia, Y., Bex, V. and Midgley, P.M. (eds.)]. Cambridge University Press, Cambridge, United Kingdom and New York, NY, USA, 2013.

Vinje, T., and Φ. Finnekåsa: The ice transport through Fram Strait, Norsk Polarinstitutt Skrifter, 186, Norwegian Polar Ins., Skrifter Series, 1986.

Vinje, T., Nordlund, N., and Kvambekk, Å.: Monitoring ice thickness in Fram Strait, J. Geophys. Res., 103(C5), 10,437–10,449, 1998.

Yang, S., and Christensen, J. H. : Arctic sea ice reduction and European cold winters in CMIP5 climate change experiments, Geophys. Res. Lett., 39, L20707, doi:10.1029/2012GL053338, 2012.

Yang, Q., Losa, S. N., Losch, M., Jung, T., Nerger, L.: The role of atmospheric uncertainty in Arctic sea ice data assimilation and prediction, Q. J. R. Meteorol. Soc., doi:10.1002/qj.2523, 2015a.

Yang, Q., Losa, S. N., Losch, M., Liu, J., Zhang, Z., Nerger, L., and Yang, H.: Assimilating summer sea ice concentration into a coupled ice-ocean model using a localized SEIK filter, Ann. Glaciol., 56(69), doi: 10.3189/2015AoG69A740, 2015b.

Zygmuntowska, M., Rampal, P., Ivanova, N., and Smedsrud, L. H.: Uncertainties in Arctic sea ice thickness and volume: new estimates and implications for trends, The Cryosphere, 8, 705-720, doi:10.5194/tc-8-705-2014, 2014.

Table 1. RMSE of the four forecasting experiments from grid-cell mean ice thickness calculated by the ULS moorings BGEP_2009A, BGEP_2009D, IMB-2010B and the satellite ice concentration observations. The two values refer to the calculation using two different data sets SICCI-NSIDC.

		BGEP_2009A	BGEP_2009D	IMB-2010B
1	MITgcm	0.87-0.90 m	0.94-0.98 m	0.91-0.91 m
2	LSEIK-1	0.45-0.49 m	0.57-0.60 m	0.54-0.52 m
3	LSEIK-2	0.61-0.64 m	0.52-0.56 m	0.73-0.70 m
4	LSEIK-3	0.45-0.48 m	0.61-0.64 m	0.51-0.47 m

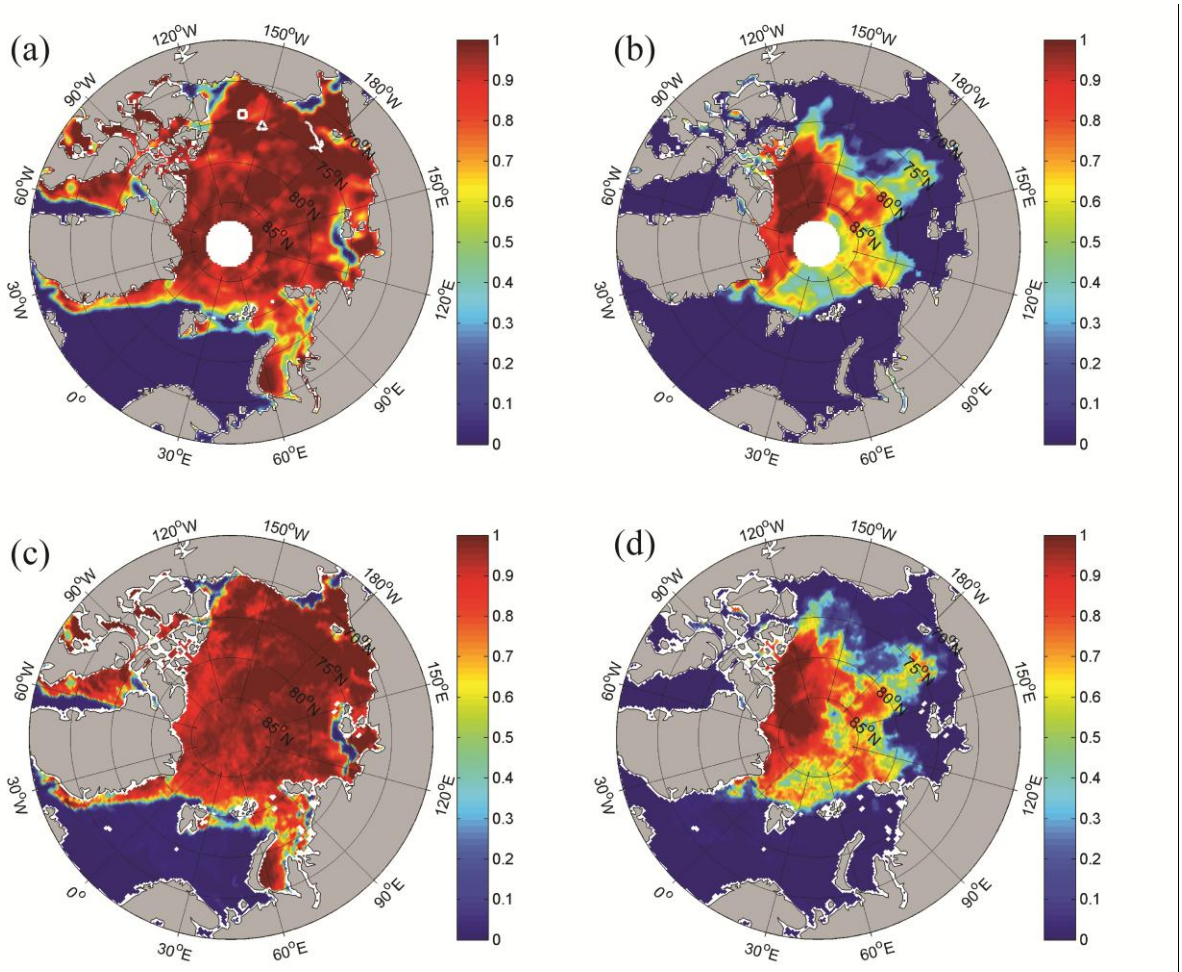

Figure 1. The NSIDC (a, b) and SICCI (c, d) sea ice concentration on 1 June (a, c) and 30 August 2010 (b, d). The locations of BGEP_2009A, BGEP_2009D and IMB_2010B are shown as a white triangle, a white square and a white line respectively.

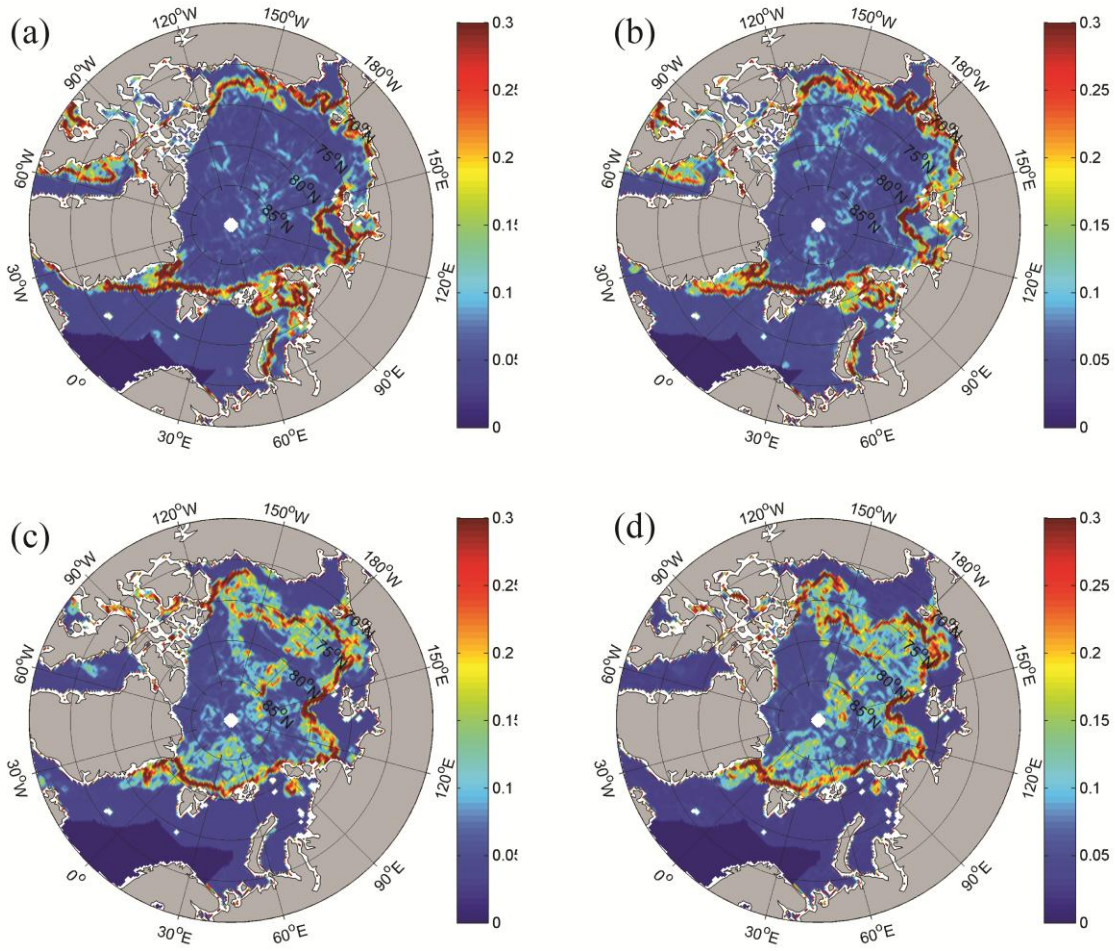

Figure 2. The uncertainty provided with SICCI sea ice concentration data on 12 July (a), 20 July (b), 13 August (c), and 21 August (d), 2010.

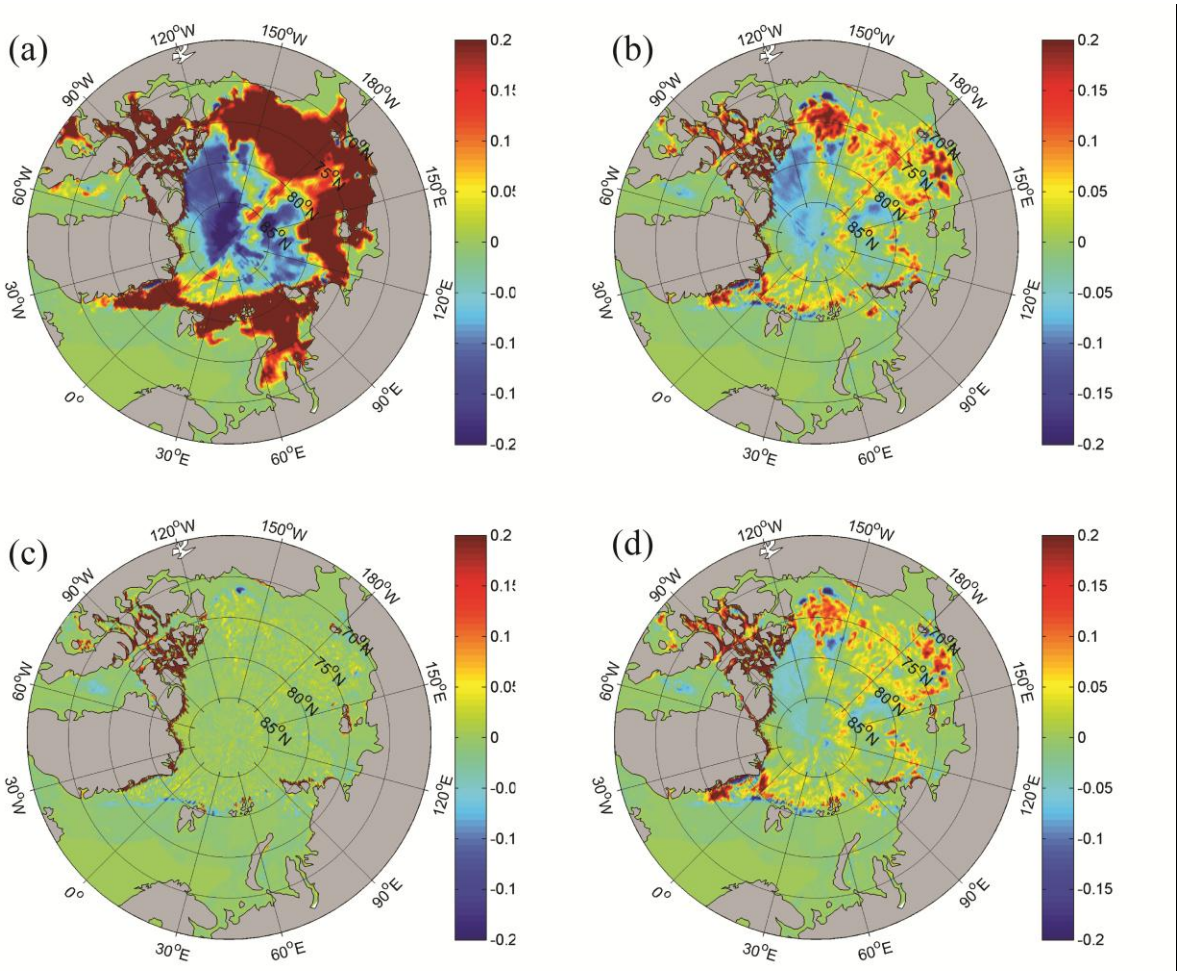

Figure 3. The forecast skill improvement of sea-ice concentration: "forecast–minus-data" averaged over August 2010. MITgcm only (a), LSEIK-1 (b), LSEIK-2 (c), and LSEIK-3 (d) 24 hour forecast minus SICCI ice concentration.

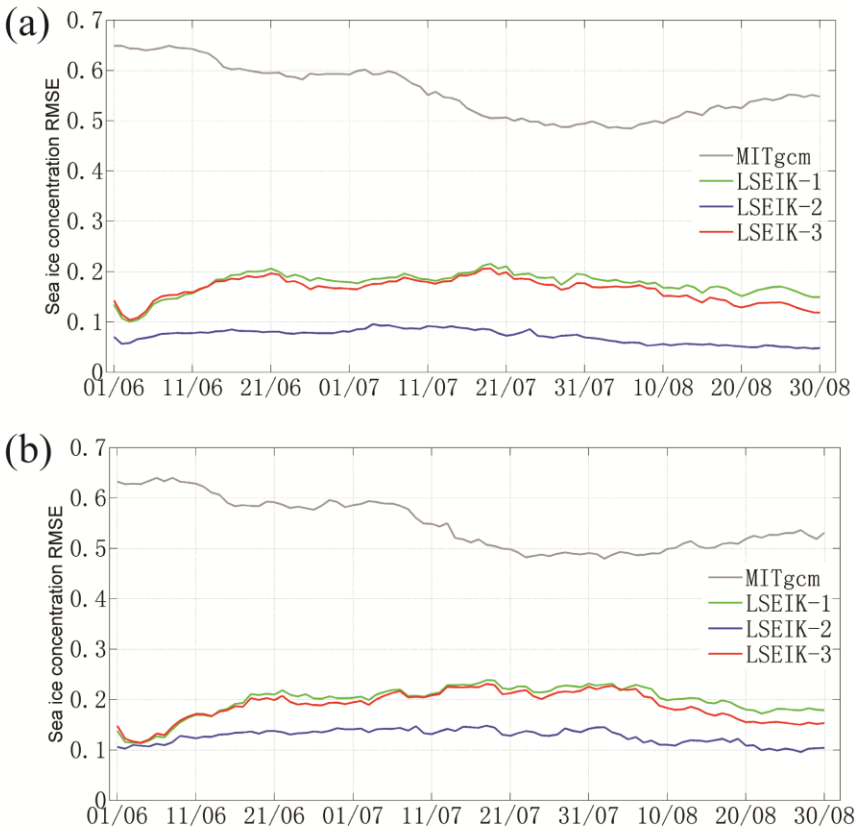

Figure 4.Temporal evolution of RMSE differences between sea ice concentration forecasts and the SICCI (a) and NSIDC (b) ice concentration data. The RMSE of the MITgcm free-run, LSEIK-1, LSEIK-2 and LSEIK-3 24-h forecasts are shown as gray, green, blue and red solid lines, respectively.

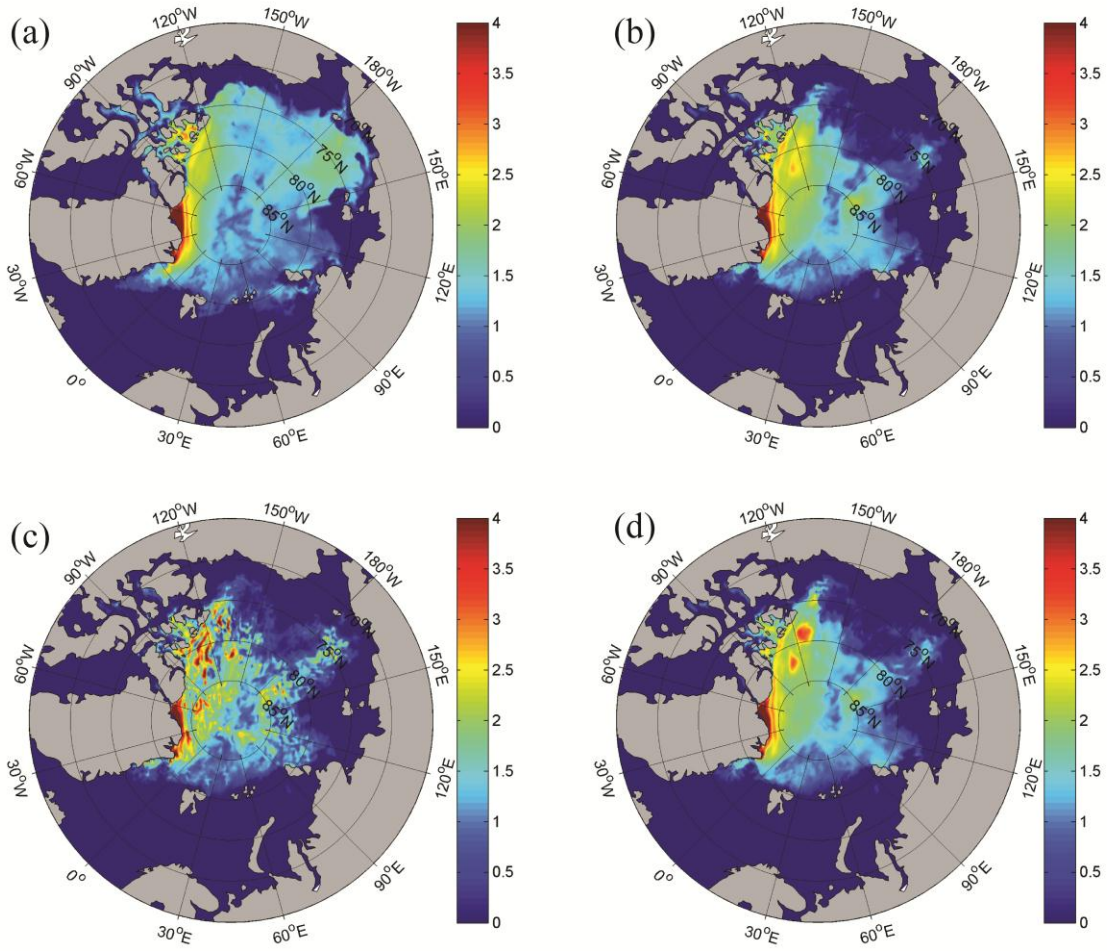

Figure 5. Sea ice thickness 24-hour forecast on August 30, 2010. MITgcm only (a), LSEIK-1 (b), LSEIK-2 (c), and LSEIK-3 (d).

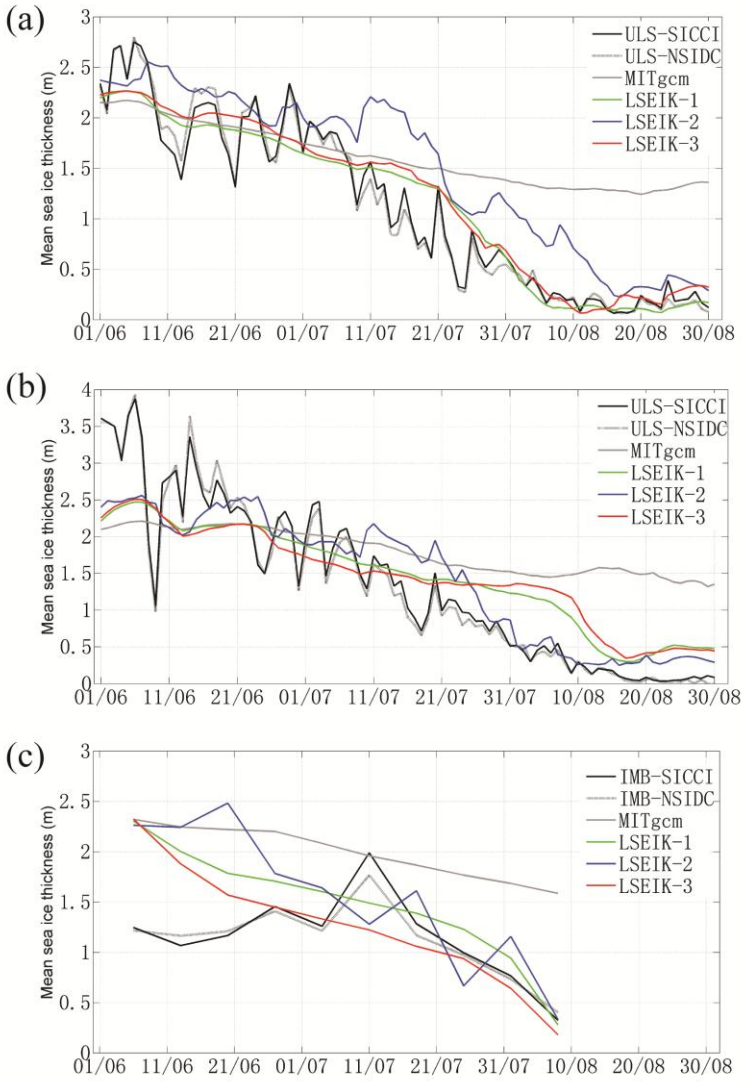

Figure 6. Evolution of grid-cell mean sea ice thickness (m) at BGEP_2009A (a), BGEP_2009D (b), and IMB_2010B (c) from 1 June to 30 August 2010. The black solid and dashed lines show the obtained grid-cell mean ice thickness using SICCI and NSIDC sea ice concentrations, respectively. The MITgcm free-run, LSEIK-1, LSEIK-2 and LSEIK-3 24 h ice thickness forecasts are shown as gray, green, blue and red solid lines, respectively.

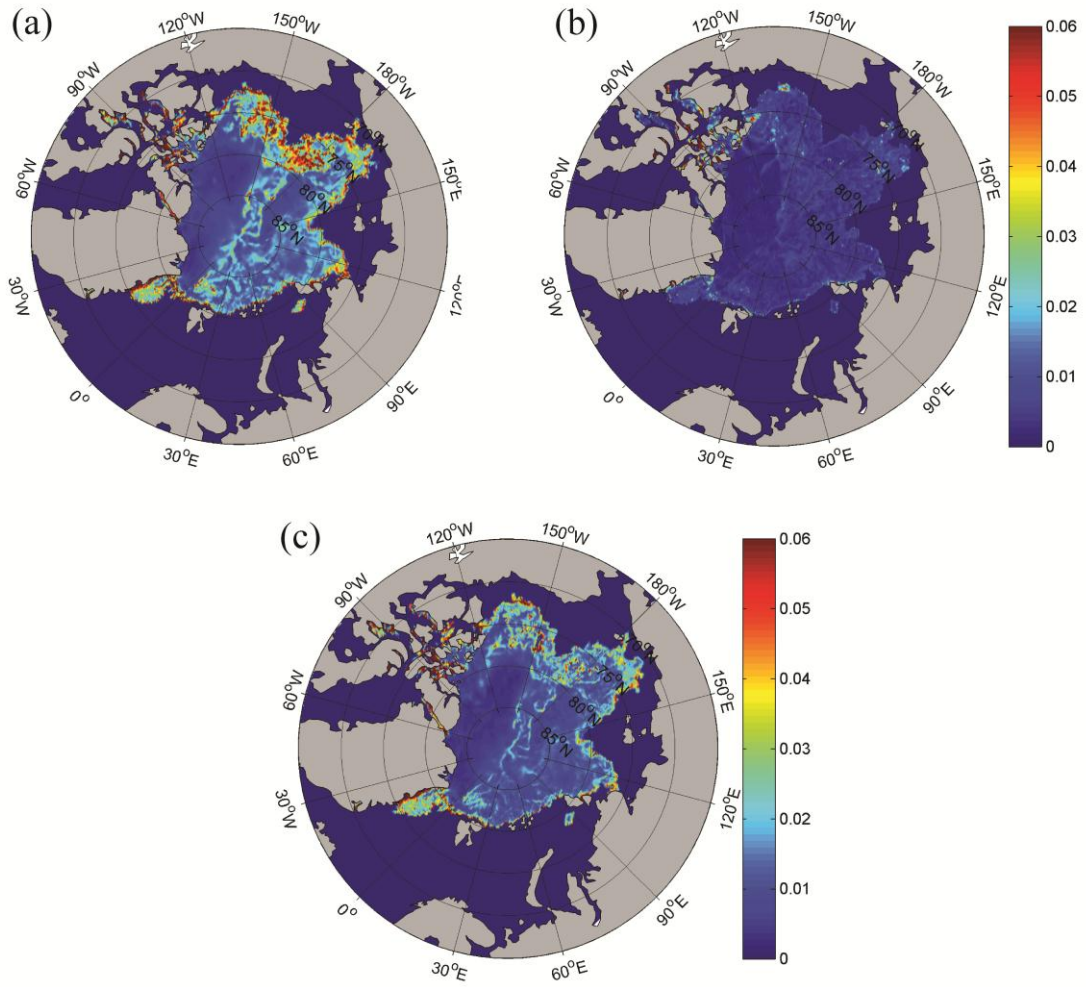

Figure 7. The ensemble spread: sea ice-concentration standard deviation for the individual grid cells as calculated from the 24-h ensemble forecasts on 30 August 2010. LSEIK-1 (a), LSEIK-2 (b), and (c) LSEIK-3 (c).

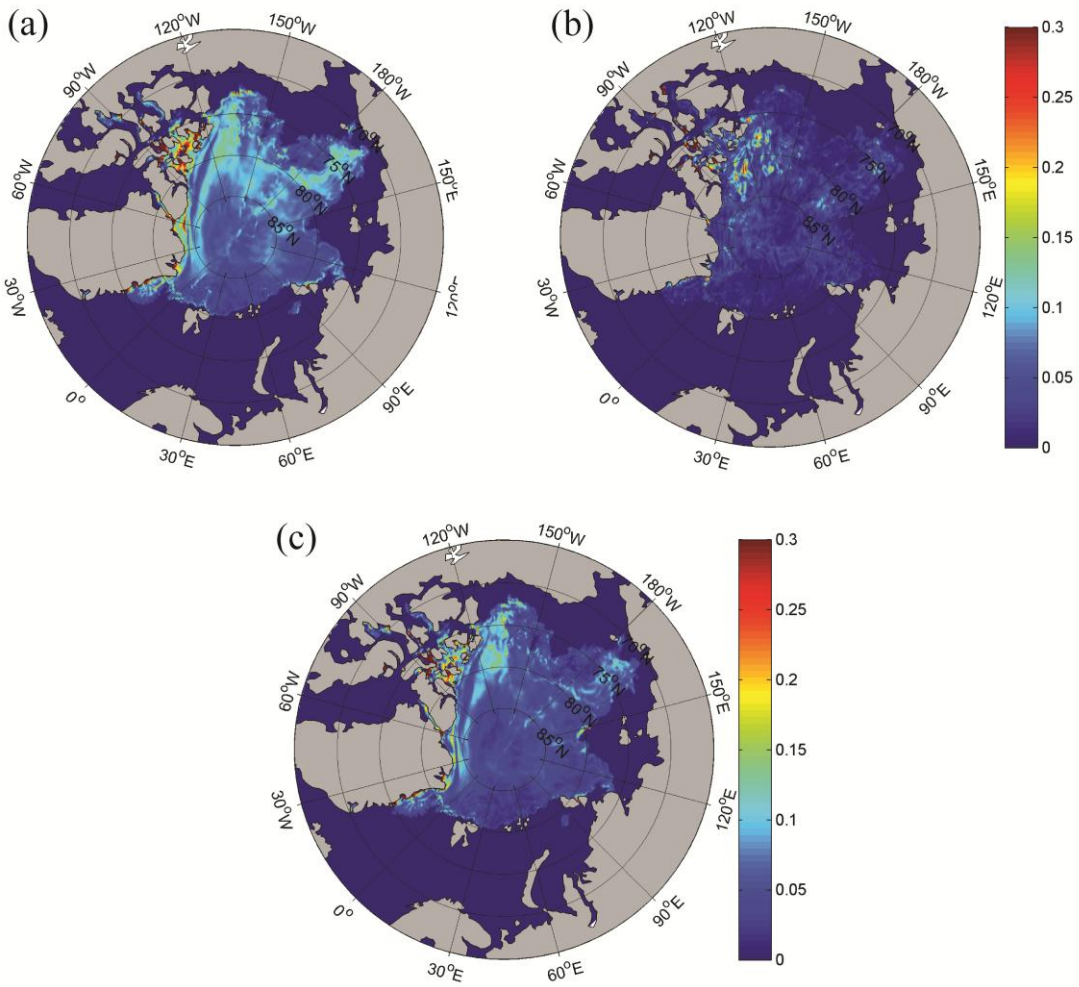

Figure 8. The ensemble spread: sea ice thickness standard deviation for the individual grid cells as calculated from the 24-h ensemble forecasts on 30 August 2010. LSEIK-1 (a), LSEIK-2 (b), and LSEIK-3 (c).

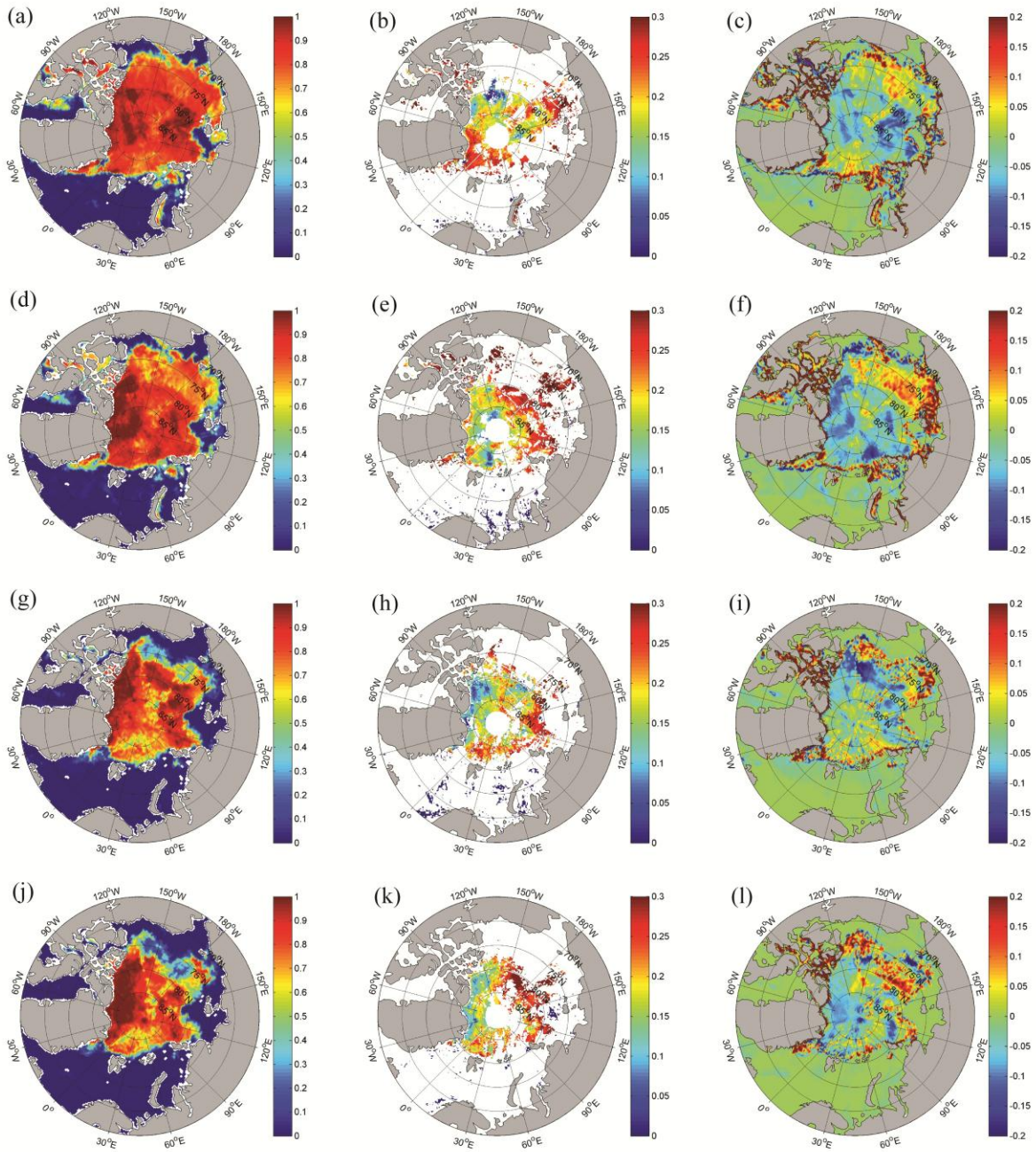

Figure 9. The SICCI sea ice concentration (left panels), the melt pond fraction (middle panels), and the LSEIK-3 forecast skill improvement of sea-ice concentration (LSEIK-3 minus SICCI; right panels), the figures from top to bottom are 12 July, 20 July, 13 August, and 21 August, 2010, respectively.